Applied Mechanics and Materials *Online: 2016-07-25*
ISSN: 1662-7482, Vol. 846, pp 300-305
doi:10.4028/www.scientific.net/AMM.846.300

Numerical Analysis of Normal Contact Stiffness of Rough Surfaces

Chongpu Zhai[1, a *], Yixiang Gan[1,b] and Dorian Hanaor[1,c]

[1]School of Civil Engineering, The University of Sydney, Sydney, Australia.

[a]c.zhai@sydney.edu.au, [b]yixiang.gan@sydney.edu.au, [c]dorian.hanaor@sydney.edu.au

Keywords: Computational contact mechanics, surface roughness, contact stiffness, fractal dimension.

Abstract. A numerical model was proposed to investigate the contact behaviour of a solid with a rough surface squeezed against a rigid flat plane. We considered simulated hierarchical surface structures as well as scanned surface data obtained by the profilometry of isotropically roughened specimens. The simulated and treated surfaces were characterised using statistical and fractal parameters. The evolution of contact stiffness under increasing normal compression was analysed through the total truncated area at varying heights, in order to relate contact mechanics to different surface parameters employed for surface characterisation. For a relatively small surface interference, the predicted stress-dependent normal contact stiffness of both scanned and simulated surfaces is in good agreement with experimental observation from nanoindentation tests, revealing a power-law function of the normal load, with the exponent of this relationship closely depending on the fractal dimension of rough surfaces. The numerical results show that the amplitude of a fractal rough surface mainly contributes to the magnitude of the contact stiffness at a given normal load.

Introduction

Rough surface morphology plays a considerable role in friction, wear, lubrication and thermal and electrical conductance. Investigations have been conducted extensively regarding the normal interfacial stiffness theoretically and experimentally [1, 2]. The pioneering works of Greenwood and Williamson [3], Bush*, et al.* [4], and Chang*, et al.* [5] were based on the contact behaviour of a single asperity and the statistical distribution of multiple asperity contacts. Considering the fractal geometry of rough surfaces, Yan and Komvopoulos [6] proposed a general contact model, revealing the variation of the contact force and real contact area during quasi-static loading. Jiang*, et al.* [7] further developed this fractal contact model, showing that experimental data (contacts between rough surfaces of the machined plane joints) is consistent with the theoretical contact stiffness. Pohrt and Popov [8]deduced a contact stiffness model for rough surfaces by means of the boundary element method. The true interfacial contact area along with roughness parameters could, at some level, be utilised to interpret the interfacial behaviour, such as the contact stiffness, electrical and thermal conductance of rough surfaces subjected to an applied normal load. However, most natural surfaces exhibit features across a wide range of length scales, involving complex morphologies and geometries, which increase the difficulties in the modelling of interfacial contact area.

Several related experiments have also been conducted on rough surfaces to obtain relationships between surface roughness parameters, loading conditions, and interfacial behaviour using a variety of microscopic approaches and a range of materials. Buzio*, et al.* [9] employed atomic force microscopy (AFM) to explore the role of surface morphology in contact mechanics at the nanoscale. Lorenz and Persson [10] presented the contact properties for an elastic block (silicon rubber) squeezed against a rigid rough substrate (an asphalt road surface). Mulvihill*, et al.* [11] applied digital image correlation and ultrasound techniques to measure the contact stiffness of real engineering interfaces. However, existing experimental and theoretical results of structure-dependent contact mechanics at rough surfaces with random multiscale features remain limited. The comparison of various reported models shows certain differences and discrepancies between analytical and experimental results [12].

The main objectives of this research are to propose a comprehensive contact mechanics analysis of rough surfaces that can be characterised by three-dimensional fractal topography and to present

numerical results interpreting the variation of contact stiffness under different loading conditions and surface characteristics.

Experimental and Theoretical Background

Scanned Surfaces. In this paper, we considered round disk samples (25 mm in diameter) made of aluminium alloy 5005 that had been subjected to surface mechanical attrition treatment (SMAT). SMAT alters surface features physically using an excitation mechanism to accelerate smooth steel balls and project them on the prepared sample surfaces [13]. We applied five-minute SMAT processes on polished surfaces using steel balls of ~1 mm in diameter, in order to modify the surface details homogeneously and isotropically. Fig. 1*a* shows a typical three-dimensional topographical map (1024×1024 pixels over a scanning area of 1×1 mm^2) of the SMATed surfaces (roughened using the aforementioned SMAT process), which was obtained by means of an optical surface profilometer (NanoMap 1000WLI). Over 10 digitized scans, the SMATed sample surfaces were characterised through the peak-valley height R_t and roll-off wavelength W_r [1], corresponding to 8.01 ± 1.474 μm and 225 ± 20.0 μm, as shown in Table 1. The differential box-counting approach was applied to calculate the fractal dimension, resulting in a value of 2.33 ± 0.0463 [14].

Simulated surfaces. The scale-invariant parameter, i.e., fractal dimension, provides a means of describing realistic multiscale roughness. Previous studies [6, 7, 15] have shown that a fractal rough surface can be deterministically simulated by the Weierstrass–Mandelbrot fractal function [16], which can be written as

$$z(x,y)=(W_r)^{(3-D_{in})}\left(\frac{\ln\gamma}{M}\right)^{1/2}\sum_{m=1}^{M}\sum_{n=0}^{n_{max}}\left(\gamma^{(D-3)n}\right)\left\{\cos\alpha_{m,n}-\cos\left[\frac{2\pi\gamma^n(x^2+y^2)^{1/2}}{W_r}\cos\left(\tan^{-1}\left(\frac{y}{x}\right)-\frac{\pi m}{M}\right)+\alpha_{m,n}\right]\right\}. \quad (1)$$

The paramter γ determines the density of the frequencies used to construct the surface and, in similarity to previous work [17, 18], is chosen to be 1.5, based on considerations of the surface flatness and frequency distribution density. The parameter W_r is the roll-off wavelength in the power spectrum, determining the basic wavelength constructing the surface. The frequency index n_{max} assumes finite values corresponding to the cut-off wavelength of the power spectrum, which is described by $\gamma^{n_{max}} = W_c$, with W_c equaling the smallest distance between two adjacent pixels [6, 15]. The prescribed fractal dimension D_{in}, which determines the slope of the log-log plot of the power spectrum of the simulated surface, is re-evaluated by differential box-counting method, which is widely used in the calculation of fractal dimension. Even though the differential box-counting method and power spectrum analysis result in different values of fractal dimension, a larger D_{in} leads to a larger D obtained in differential box-counting approach, corresponding to denser roughness. The parameter M denotes the number of superposed ridges used to construct the surface. A random number generator is used to uniformly distribute the values of random phase $\alpha_{m,n}$. Here, five isotropic fractal surfaces, consisting of 1024×1024 pixels, were generated to simulate SMATed surfaces based on the surface descriptors obtained from digitised scans. Input values for surface simulation were chosen as $M = 10$, $D_{in} = 2.15$ and $W_r = 225$. The values of all pixels, representing the height, were then scaled according to the height-width ratio (R_t/L, where L is the side length of the surface, equalling 1 mm) of the simulated surface, in order to yield a peak-valley height of R_t =8 μm.

Table 1: Surface characterisation for SMATed surfaces and simulated surfaces

Surface	Peak-valley height, R_t	Roll-off wavelength, W_r	Fractal dimension, D
SMATed	8.01 ± 1.474 μm	225 ± 22.5 μm	2.33 ± 0.0463
Simulated	8 μm	225 μm	2.36 ± 0.0297

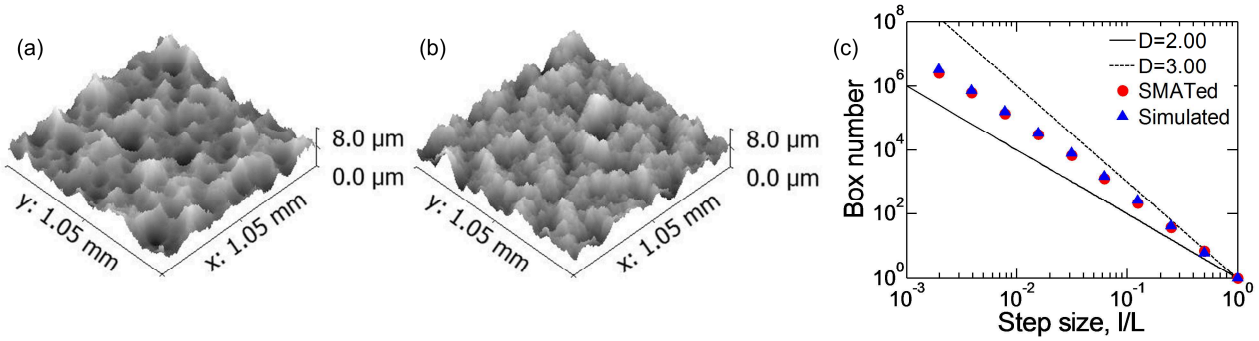

Fig. 1: (a) A typical profilometer scan of the SMATed surface; (b) the simulated fractal surface; (c) log-log plots of box number and normalized step size for a typical scanned surface and a typical simulated surface.

From the analysis of simulated surfaces, the mean fractality averaged over ten surfaces was found as and D =2.36 ± 0.0297. The prescribed values (R_t and W_r) and evaluated values (D) of surface roughness descriptors are in close agreement with those of the SMATed surface, as indicated in Table 1. The box numbers with respect to the step size, for both the scanned and simulated surfaces, are illustrated in Fig. 1c, based on cross-scale comparison.

Contact modelling. True contact between rough surfaces involves only a small fraction of the nominal contact area. Contacting surface asperities may deform elastically or plastically, depending on material properties and loading conditions. In this research we assume that the truncated surface features on the rough surfaces flow into the valleys of non-contacting regions. This is reasonable for relatively low contact loads. We consider a simple extension of the contact analysis for the indentation of an elastic half space [19, 20], which reveals that there is a geometry independent relation among contact stiffness, contact area, and elastic modulus, given by

$$E_r = \frac{\sqrt{\pi}}{2}\frac{k}{\sqrt{A_T}}, \tag{2}$$

where k is the surface stiffness in the unit of N/m, $A_T = \sum_{i=1}^{i=n} A_i$ is the summation of areas of all contacting asperities. The reduced elastic modulus E_r, including contributions from the compressed rough surface E_c and the opposing flat surface E_i, is given by $1/E_r = (1-v_c^2)/E_c + (1-v_i^2)/E_i$, with the subscript i indicating the property of the opposing surface, the subscript c indicating the properties of the compressed surface and υ being the Poisson's ratio. Eq. 2 is a fundamental equation for assessing the elastic properties in indentation tests, and has been shown to be equally applicable in cases of elastic-plastic contact. If the elastic modulus is known, the relationship between contact area and contact stiffness can be obtained [19, 20]. Note that smaller microcontacts merge to form larger ones and the value of contact stiffness E_c approaches the elastic modulus of the surface material, E, as the load increases. Thus, the contact stiffness E_c can be given by $E_c = \left(E_r'\sqrt{A_T}\right)/\sqrt{A_p}$, where A_p is the projected area of the simulated surface under compression. E_r' can be determined from the expression $1/E_r' = (1-v^2)/E + (1-v_i^2)/E_i$. Considering $\mathrm{d}F = k(\omega)\mathrm{d}\omega$, we can then obtain the loading force F through integration during the compression with penetration increments $\mathrm{d}\omega$.

In this model, for a given surface interference ω, the total contact area under compression is simply determined from numerical integration of the truncated areas of the rough surface, at corresponding truncation height, $h = Rt - \omega$. The contours of the truncated islands at varying heights for the scanned SMATed surface and a simulated surface are shown in Fig. 2. Based on the theory of Mandelbrot [16], Yan and Komvopoulos [6] proposed that the total truncated area is related to the largest truncated island area A_{max} and the fractal dimension. The truncated asperity size distribution function can be written as

$$n(\mathrm{A}) = \frac{D-1}{2A_{\max}}\left(\frac{A_{\max}}{A}\right)^{(D+1)/2} . \quad (3)$$

For both the scanned and simulated surfaces, we have analysed size distributions of the truncated areas and compared the fitted curves of the size probability distribution with the theoretical prediction, as illustrated in Fig. 2*c*.

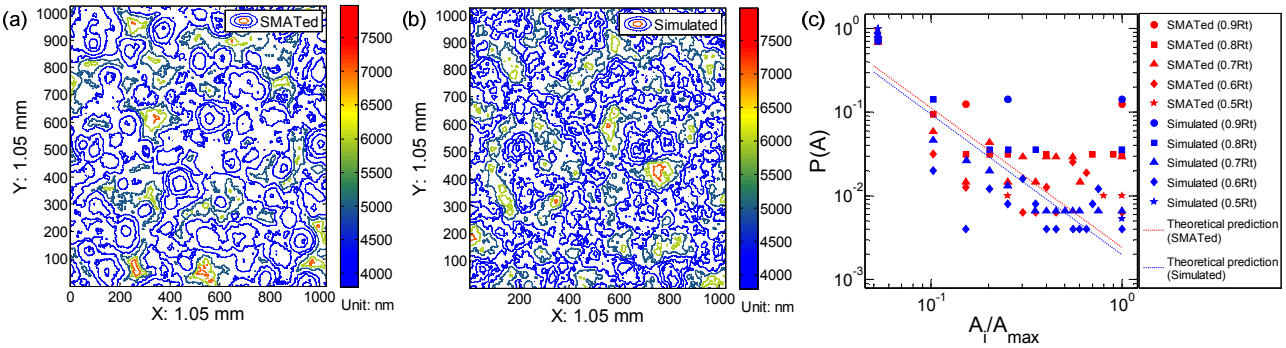

Fig. 2: (a) Contours of truncated islands of a typical scan from the SMATed surface at varying heights; (b) contours of truncated islands of the simulated surface at varying heights; (c) the probability distribution of the size of truncated islands at varying heights for a typical scanned surface and a typical simulated surface, compared with theoretical predications.

Verification of the Contact Model Predictions

The normal contact stiffness of the SMATed surface was evaluated through flat-tipped diamond nanoindentation tests employing the partial unloading method. Three indenter tips of various diameters, 54.1 μm, 108.7 μm, and 502.6 μm (SYNTON-MDP, FLT-D050, FLT-D100, and FLT-D500), were employed in order to acquire data across a wide range of stress levels (0.05 MPa to 214 MPa). Stiffness values at different stress levels were determined by averaging over 10 indentation tests at different positions on the treated surface. To compare the measured contact stiffness with the numerical results of the scanned and simulated surfaces, we converted the obtained unloading stiffness $k' = \mathrm{d}P/\mathrm{d}S$, where P designates the load and S is the indentation depth, to the contact stiffness E_c (in units of N/m^2) through $E_r = \left(\sqrt{\pi}k'\right)/\left(2\sqrt{A_P}\right)$, where A_P is the projected area of the indenter tip. The non-dimensional stress is defined as $F/(EA_P)$. Similarly, for the numerical analyses of scanned and simulated surfaces, the compression force F is non-dimensionalised as $F/(EA_p)$.

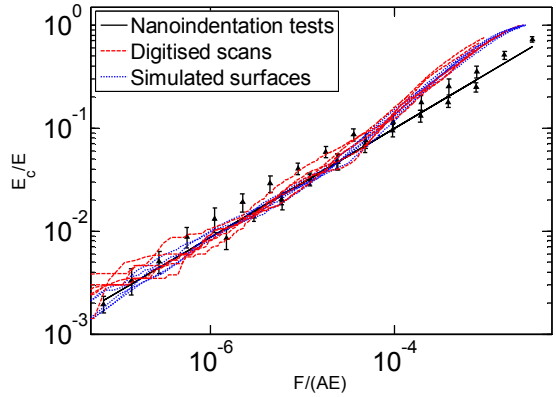

Fig. 3: The normal contact stiffness as a function of the normal pressure, obtained with nanoindentation tests and numerical analyses of scanned and simulated surfaces.

The experimental results from nanoindentation and the calculated contact stiffness of the scanned and simulated SMATed surfaces (with the largest surface interference being 0.7Rt) are shown in Fig. 3. Only the results of five scanned surfaces (out of 10 scans of SMATed surface at

various postions) and five simulated surfaces are provided in Fig. 3 for greater clarity. The comparison between the contact stiffness obtained from scanned surfaces and the experimental results indicates that the present contact model for evaluating the contact stiffness is appropriate for relatively small loads. However, discrepancies increase towards higher values of loading force and surface interference. It can be seen clearly that the results of simulated surfaces agree well with the scanned surfaces, showing the capability and repeatability of this model to evaluate the contact properties based on surface roughness parameters, including the peak-valley height, roll-off wavelength, and fractal dimension.

Applications and Discussions

From the normalised data shown in Fig. 3, we find that the contact stiffness of a rough surface compressed by a rigid flat plane exhibits a power-law relationship with the applied normal load, which can be described as $E_c/E = \beta[F/(EA)]^{\alpha}$. The parameters of exponent α and magnitude β are assumed to be constant for a given surface structure. Two groups of surfaces (1024×1024 pixels over an area of 1×1 mm^2) were generated and analysed by the present model, with the maximum surface interference being $0.1Rt$. One group of simulated surfaces have the same relative roughness amplitude, described as $\delta = R_t/W_r = 0.04$ and varying D_{in} (2.10, 2.30, 2.50, 2.70, and 2.90). For the other group, the surface fractal dimension D_{in} was set as 2.50 and the roughness amplitude δ was varied (0.01, 0.02, 0.04, 0.08, 0.16). In order to further test the repeatability of the present model, we analysed five simulated surfaces for each individual set of input parameters. The results are shown in Fig. 4. It can be seen clearly that (1) the exponent α increases with values of fractal dimension, and (2) the roughness amplitude, δ, indicating primarily the vertical scale of the rough surface, dominates β. Similar formulas have been used as the theoretical approximation for the contact stiffness from Yan and Komvopoulos [6], Jiang, *et al.* [7], and Pohrt and Popov [8]. In all these theories, the relationship between the stiffness and pressure was found to follow a power law, with the exponent strongly correlated to the value of fractal dimension. The fitting functions for the stiffness parameters, i.e., α and β, using Ra and D_{in} were obtained, expressed as $\alpha = 0.875D - 1.63$ and $\beta = 5.81(\delta)^{-0.786}$.

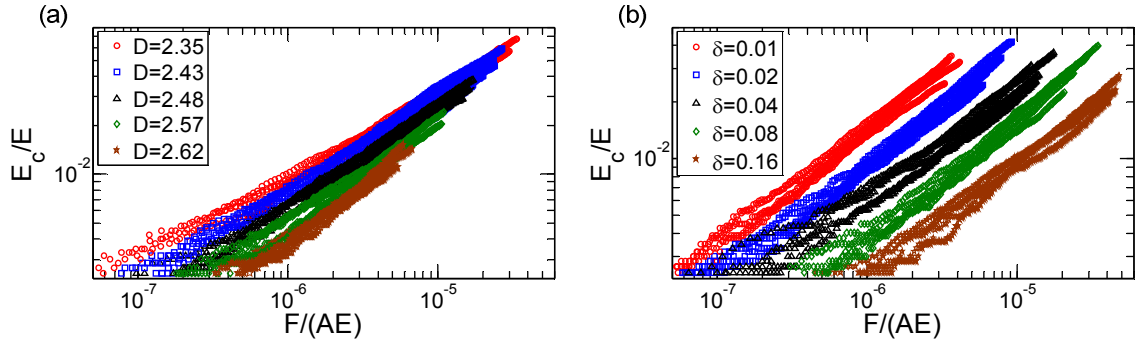

Fig. 4: Dependence of the normal contact stiffness on the normal pressure: (a) with same value of $\delta = 40$ and differenct D_{in}; (b) with same value of $D_{in} = 2.5$ and different δ.

Conclusion

A simplified numerical model for the analysis of the normal contact stiffness of rough surfaces compressed by rigid flat planes was presented. A contact model has been proposed to predict the contact stiffness based on the truncated areas of contacting rough surfaces. This model was employed to analyse contact behaviour of real and simulated surface structures exhibiting similar roughness characteristics yielding results that were in good agreement with experimental data obtained from flat tipped nanoindentation tests. The present methodology facilitates the analysis of the relationship of contact stiffness with applied load for varied surface descriptors including peak-valley height, roll-off wavelength, and fractal dimension. This relationship is then simplified

through a power-law expression as $E_c/E = \beta[F/(EA)]^{\alpha}$, with the exponent α being correlated to the fractal dimension of the surface and the coefficient β being dominated by surfaces' relative roughness amplitude. This contact model provides an efficient approach to investigating the contact properties at rough interfaces.

Acknowledgement: Financial support for this research from the Australian Research Council through grants DE130101639 is greatly appreciated.

References

[1] B. Persson, O. Albohr, U. Tartaglino, A. Volokitin, E. Tosatti, On the nature of surface roughness with application to contact mechanics, sealing, rubber friction and adhesion, Journal of Physics: Condensed Matter, 17 (2005) R1.
[2] V.L. Popov, Contact mechanics and friction, Springer Science & Business Media, Berlin, 2010.
[3] J. Greenwood, J. Williamson, Contact of nominally flat surfaces, Proceedings of the Royal Society of London. Series A. Mathematical and Physical Sciences, 295 (1966) 300-319.
[4] A. Bush, R. Gibson, T. Thomas, The elastic contact of a rough surface, Wear, 35 (1975) 87-111.
[5] W. Chang, I. Etsion, D.B. Bogy, An elastic-plastic model for the contact of rough surfaces, Journal of tribology, 109 (1987) 257-263.
[6] W. Yan, K. Komvopoulos, Contact analysis of elastic-plastic fractal surfaces, Journal of Applied Physics, 84 (1998) 3617-3624.
[7] S. Jiang, Y. Zheng, H. Zhu, A contact stiffness model of machined plane joint based on fractal theory, Journal of Tribology, 132 (2010) 011401.
[8] R. Pohrt, V.L. Popov, Normal contact stiffness of elastic solids with fractal rough surfaces, Physical Review Letters, 108 (2012) 104301.
[9] R. Buzio, C. Boragno, F. Biscarini, F.B. De Mongeot, U. Valbusa, The contact mechanics of fractal surfaces, Nature Materials, 2 (2003) 233-236.
[10] B. Lorenz, B. Persson, Interfacial separation between elastic solids with randomly rough surfaces: comparison of experiment with theory, Journal of Physics: Condensed Matter, 21 (2009) 015003.
[11] D. Mulvihill, H. Brunskill, M. Kartal, R. Dwyer-Joyce, D. Nowell, A comparison of contact stiffness measurements obtained by the digital image correlation and ultrasound techniques, Experimental Mechanics, 53 (2013) 1245-1263.
[12] G. Carbone, F. Bottiglione, Asperity contact theories: Do they predict linearity between contact area and load?, Journal of the Mechanics and Physics of Solids, 56 (2008) 2555-2572.
[13] C. Zhai, D. Hanaor, G. Proust, Y. Gan, Stress-Dependent Electrical Contact Resistance at Fractal Rough Surfaces, Journal of Engineering Mechanics, (2015) B4015001.
[14] H. Xie, J.-a. Wang, Direct fractal measurement of fracture surfaces, International Journal of Solids and Structures, 36 (1999) 3073-3084.
[15] P. Liu, H. Zhao, K. Huang, Q. Chen, Research on normal contact stiffness of rough surface considering friction based on fractal theory, Applied Surface Science, 349 (2015) 43-48.
[16] B.B. Mandelbrot, The fractal geometry of nature, Macmillan, 1983.
[17] D.A. Hanaor, Y. Gan, I. Einav, Effects of surface structure deformation on static friction at fractal interfaces, Geotechnique Letters, 3 (2013) 52-58.
[18] L. Kogut, R.L. Jackson, A comparison of contact modeling utilizing statistical and fractal approaches, Journal of tribology, 128 (2006) 213-217.
[19] G. Pharr, W. Oliver, F. Brotzen, On the generality of the relationship among contact stiffness, contact area, and elastic modulus during indentation, Journal of materials research, 7 (1992) 613-617.
[20] W.C. Oliver, G.M. Pharr, Measurement of hardness and elastic modulus by instrumented indentation: Advances in understanding and refinements to methodology, Journal of Materials Research, 19 (2004) 3-20.